



Thermal transport in planar sp²-hybridized carbon allotropes: A comparative study of biphenylene network, pentaheptite and graphene



Penghua Ying^{a,1}, Ting Liang^{b,1}, Yao Du^a, Jin Zhang^{a,*}, Xiaoliang Zeng^b, Zheng Zhong^{a,*}

^a School of Science, Harbin Institute of Technology, Shenzhen 518055, PR China

^b Shenzhen Institute of Advanced Electronic Materials, Shenzhen Institute of Advanced Technology, Chinese Academy of Sciences, Shenzhen 518055, PR China

ARTICLE INFO

Article history:

Received 23 August 2021

Revised 29 September 2021

Accepted 4 October 2021

Available online 10 October 2021

Keywords:

Biphenylene network

Planar carbon allotropes

Thermal conductivity

Molecular dynamics

Phonon transport

ABSTRACT

The biphenylene network with periodically arranged four-, six-, and eight-membered rings has been successfully synthesized in very recent experiments. This novel two-dimensional (2D) carbon allotrope has potentials in applications of lithium storage and carbon-based circuitry. Understanding the thermal transport properties of biphenylene network is of critical importance for the performance and reliability of its practical applications. To this end, the thermal transport in biphenylene network is comprehensively investigated in this paper with the aid of molecular dynamics simulations together with first-principles calculations. For the sake of comparison, the thermal conductivities of other 2D sp²-hybridized carbon allotropes including graphene and pentaheptite are also investigated using the same method. It is found that the thermal conductivities of biphenylene network and pentaheptite are, respectively, only about one-thirteenth and one-eighth of graphene. Through the analysis of phonon property, mechanical property and electron density distribution, it is demonstrated that the great reduction in the thermal conductivity of biphenylene network and pentaheptite arises from the decline in their structural symmetry, which leads to the decrease of phonon group velocity and the reduction of phonon mean free path.

© 2021 Published by Elsevier Ltd.

1. Introduction

Since Geim and Novoselov experimentally discovered graphene by using micromechanical cleavage in 2004 [1], this two-dimensional (2D) carbon allotrope has attracted a great amount of interest in academia and industry by virtue of its superior and novel physical properties. For example, previous experiments demonstrated that graphene has an ultrahigh strength of 130 GPa, a large Young's modulus up to 1 TPa [2], and an extremely high thermal conductivity in the range of 3000–5800 W/(mK) [3,4]. Inspired by the extraordinary structural and material properties observed in graphene, numerous 2D materials based on other elements have also been reported, such as hexagonal boron nitride, transition metal dichalcogenides (e.g., MoS₂ and MoTe₂), and many monoelements including silicene, germanene, phosphorene, stanene and borophene [5]. In addition, the demand of other 2D carbon allotropes also stimulates substantial efforts in searching pure-carbon nanodevices beyond graphene. To date, a large amount of novel 2D carbon allotropes have been theoretically pre-

dicted with the aid of the structure searching method and first-principles calculations, though only a few have been successfully synthesized in experiments. In 2010, graphdiyne whose crystal lattice is arranged with sp and sp²-bonded carbon atoms was reported by Li and coworkers in their experimental study [6]. Very recently, Fan et al. experimentally reported the bottom-up growth of an ultraflat biphenylene network with repeating nonhexagonal motifs along both planar dimensions [7]. In addition to graphene, the biphenylene network is the second pure sp²-hybridized carbon allotrope successfully synthesized. This novel material is expected to be used in the fields of lithium storage and carbon-based circuitry [7].

Understanding the thermal transport in 2D carbon allotropes not only provides an important guidance for related applications, but also is the essential step to reveal the fundamental mechanism of phonon transport in low-dimensional systems. Theoretically, the phonon thermal conductivity can be obtained by lattice dynamic methods or molecular dynamics (MD)-based methods. By using the homogeneous non-equilibrium molecular dynamics (HNEMD) method [8], the thermal conductivity of graphene was predicted to be around 3000 W/(mK) at room temperature, which is higher than the value of any other known 2D carbon allotropes. The outstanding thermal transport property observed in graphene can be attributed to its strong sp²-hybridized bond and

* Corresponding authors.

E-mail addresses: jinzhang@hit.edu.cn (J. Zhang), zhongzheng@hit.edu.cn (Z. Zhong).

¹ These authors contributed equally.

honeycomb lattice with very high symmetry. As for other 2D carbon allotropes, their thermal conductivity is reported to be substantially smaller than that of graphene. For example, based on phonon Boltzmann transport equation (BTE) and first-principles calculations, the thermal conductivities of α , β , and γ graphyne with sp and sp^2 -hybridized bonds were predicted to be 21.1, 22.3 and 106.2 W/(mK) at room temperature, respectively, which are one order or two orders of magnitude smaller than 2962.8 W/(mK) of graphene [9]. Using the same method, the thermal conductivity of penta-graphene [10] with sp and sp^3 -hybridized bonds was predicted to be 645 W/(mK) at room temperature [11], which is also significantly smaller than that of graphene. Equilibrium molecular dynamics (EMD) simulations together with Green-Kubo method [12,13] were employed to predict the thermal conductivities of OPG-L and OPG-Z [14] with pure sp^2 -hybridized bonds, which are 313–344 W/(mK) and 233–261 W/(mK) at room temperature, respectively. Very recently, the thermal conductivities of penta-graphene (392 W/(mK)) and three pure sp^2 -hybridized 2D carbon allotropes including ψ -graphene [15] (338 W/(mK)), pop-graphene [16] (156.5 W/(mK)), and net-W [17] (156.5 W/(mK)) were obtained by extrapolating the non-equilibrium molecular dynamics (NEMD) results [18]. All previous results suggested a greatly weaker thermal transport property existing in other 2D carbon allotropes when compare with the pristine graphene.

Compared with a large number of studies reported for the thermal conductivity of graphene, the study on the thermal transport in some other 2D carbon allotropes is still limited. Especially, the newly synthesized biphenylene network [7] and the theoretically predicted pentaheptite [19] show a periodically arranged non-benzenoid structure different from the pristine honeycomb lattice in graphene. This different lattice structure is expected to result in distinct thermal transport property of biphenylene network and pentaheptite when compared to graphene. Thus, it is essential to conduct a comprehensive study on the thermal transport in these new sp^2 -hybridized 2D carbon allotropes. In addition, as mentioned above, in the previous MD calculations on the thermal transport properties of 2D carbon allotropes, the conventional EMD and NEMD methods were widely employed. However, the previous EMD method based on the multi-body potential such as Tersoff potential [20] usually heavily underestimates the per-atom stress-based heat current, which correspondingly results in an underestimation of the thermal conductivity [21]. Meanwhile, due to the boundary scattering and long mean free path (MFP) in 2D carbon allotropes, the thermal conductivity of 2D carbon allotropes extracted from previous NEMD methods were also been underestimated [8]. Thus, some new MD-based methods are required to achieve a more accurate calculation of the thermal conductivity of 2D carbon allotropes. In this work, a comparative study on the thermal transport in planar sp^2 -hybridized carbon allotropes including graphene, biphenylene network, and pentaheptite is performed by using graphics processing units molecular dynamics (GPUMD) [22] simulations. Three MD-based methods including HNEMD, EMD, and NEMD are used to predict the thermal conductivity of carbon allotropes. The spectral heat current (SHC) analysis, lattice dynamics calculations, electron localization function calculations and tensile simulations are also performed to reveal the mechanism underlying the phonon transport in these 2D carbon allotropes.

2. Model and methods

2.1. Simulation model

As shown in Fig. 1, the lattice structures of biphenylene network and pentaheptite can be obtained by reorganizing some partial bonds in graphene. Specifically, when generating the penta-

heptite, all six-membered carbon rings in graphene are equally split into five- and seven- membered carbon rings. In generating the biphenylene network, partial six-membered rings in graphene are split into four- and eight- membered carbon rings, resulting in the coexistence of ternary (four-, six-, and eight-membered) carbon rings. Here, the cell size of graphene, biphenylene network and pentaheptite is set as 25 nm \times 25 nm in all HNEMD and EMD simulations, which is sufficiently large to eliminate the finite-size effect [8]. Correspondingly, there are 24,072, 22,110, and 24,072 atoms in the present simulation models of graphene, biphenylene network, and pentaheptite, respectively. Periodic boundary conditions are applied in both planar directions, while the free boundary condition is applied in the thickness direction. Here, the principal (i.e., armchair and zigzag) directions in pentaheptite and biphenylene network are consistent with graphene, which means that the definition of armchair and zigzag directions of biphenylene network and pentaheptite keeps unchanged during the structural construction based on graphene (see dotted lines in Fig. 1(b and c)). It is noted here that only the phonon thermal conductivity of biphenylene network is considered in the present calculations. Nevertheless, according to the recent study [7], the biphenylene network could be a metallic material when it possesses a large width. Under this circumstance, the electrons may also contribute to the thermal conductivity of biphenylene network, which is worth being comprehensively discussed in the future study to achieve a more precise prediction of the thermal conductivity of biphenylene network.

2.2. Thermal conductivity calculations

All calculations of thermal conductivity based on MD simulations were performed at room temperature (300 K) using the open source GPUMD package [22], in which the standard Newton equations of motion are integrated in time by the velocity-Verlet integration algorithm [23]. Due to the more efficient algorithms and implementations, GPUMD is of higher efficiency in calculating phonon thermal conductivity when compared to any other MD codes such as LAMMPS [24]. In addition, GPUMD can correctly calculate the heat flux of multi-body potential systems, which is significantly underestimated by LAMMPS [21]. The thermal transport along both principal directions, i.e., armchair and zigzag directions were investigated for all carbon allotropes. The optimized Tersoff force field [20] was employed to describe the atomic interactions in all carbon allotropes. This force field has been widely utilized in previous MD simulations on the mechanical and thermal properties of various carbon-based 2D materials [25–29]. To examine the reliability of this force field in calculating the phonon transport in 2D carbon allotropes considered in this work, we compared the lattice lengths and energies of these 2D carbon allotropes predicted from the optimized Tersoff force field to the results calculated from first-principles calculations in Fig. S1 (see supplementary materials). It was found that the results obtained from two methods agree very well with each other. Specifically, the energies of pentaheptite and biphenylene network obtained from the optimized Tersoff potential are, respectively, 0.37 eV/atom and 0.70 eV/atom, which are consistent with the corresponding results of 0.24 eV/atom (pentaheptite) and 0.47 eV/atom (biphenylene network) obtained from first-principles calculations. The energy of pentaheptite and biphenylene network is found to be higher than that of graphene, which indicates their structure is relatively unstable compared with graphene. Therefore, to improve the calculation efficiency without losing calculation accuracy, we adopted a relatively small time step of 0.1 fs and 0.25 fs for biphenylene network and pentaheptite, respectively, while a larger time step of 0.5 fs was selected for graphene. The reliability of these selected time steps has been carefully verified as detailed in supple-

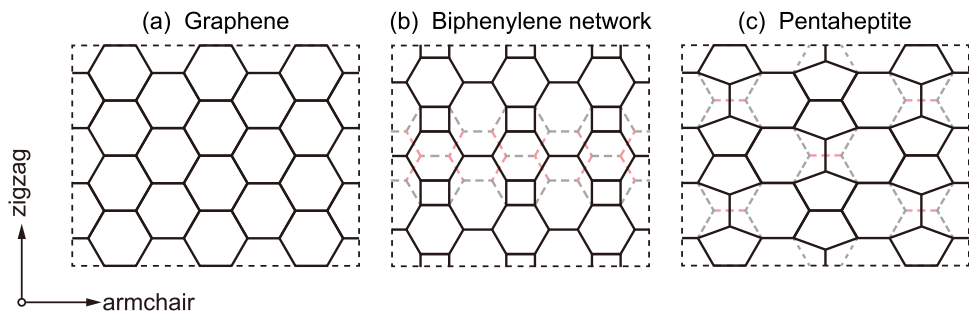


Fig. 1. Lattice structures of (a) graphene with six-membered carbon rings, (b) biphenylene network with four-, six-, and eight-membered carbon rings, and (c) pentaheptite with five- and seven-membered carbon rings.

mentary materials. As for the newly synthesized biphenylene network, we also compared its phonon dispersion relations calculated from various force fields including aforementioned optimized Tersoff, AIREBO [30], and ReaxFF [31] to the results extracted from first-principles calculations in Fig. S5 (see supplementary materials). Among three force fields, the optimized Tersoff has the highest accuracy in describing the phonon band structure for biphenylene network.

In this work, the thermal conductivities of planar carbon allotropes were calculated by three different MD-based methods including HNEMD, EMD, and NEMD. The corresponding theories and simulation details were briefly presented below.

2.2.1. HNEMD simulations

Based on the non-canonical linear response theory, Evans proposed the HNEMD method in 1982 [32], which was recently extended to general many-body potentials in GPUMD package developed by Fan and coworkers [8]. For planar carbon allotropes considered here, the thermal conductivity along armchair or zigzag direction on the basis of HNEMD simulations is given by

$$\kappa(t) = \frac{1}{t} \int_0^t \frac{\langle J(\tau) \rangle}{TVF_e} d\tau, \quad (1)$$

where t , V , and T are, respectively, the production time, system volume, and temperature. $\langle J(\tau) \rangle$ is the nonequilibrium heat current induced by the driving force and F_e is the driving force parameter. The symbol $\langle \rangle$ denotes the average over simulation time t . The volume of 2D materials usually depends on their thickness, which has diverse theoretical predictions in various literatures [33]. To avoid the influence of thickness definition and, meanwhile, to make the comparison of the thermal conductivity more direct, a conventional value of 0.335 nm was used here for the thickness of all three carbon allotropes. Previous studies demonstrated that the driving force parameter F_e should be within a reasonable range. On one hand, F_e has to be small enough to keep the system within the linear-response regime and converge within the simulation time. On the other hand, F_e has to be large enough to obtain a reliable result with a large signal-to-noise ratio [32,34,35]. According to the rule of thumb [8], the value of F_e should be roughly smaller than $1/\lambda_{\max}$, where λ_{\max} denotes the maximum MFP. Fig. 2(a and b) shows the sensitivity of $\kappa(t)$ to the parameter F_e for biphenylene network. The value of $\kappa(t)$ is found to diverge with increasing t when $F_e \geq 0.6 \mu\text{m}^{-1}$, and converge when $F_e \leq 0.5 \mu\text{m}^{-1}$. However, a very small value $F_e = 0.05 \mu\text{m}^{-1}$ would result in a significant noise. Under this circumstance, more simulations are needed to obtain a more reliable value of $\kappa(t)$. Based on the above analyses, $F_e = 0.1 \mu\text{m}^{-1}$ was applied for all carbon allotropes considered in this work, which is consistent with the value selected in the previous HNEMD simulations of graphene [8] and polyaniline (C_3N) [26].

The energy minimization was performed to the initial models of all carbon allotropes as shown in Fig. 1. After that, the samples were relaxed in the NPT ensemble (constant number of particles, pressure, and temperature) with zero pressure and, subsequently, in the NVT ensemble (constant number of particles, volume, and temperature) to obtain the equilibrium configurations. The Nosé-Hoover barostat and thermostat methods were employed to control the temperature and pressure of the simulation box. A total simulation time of 10 ns was used to obtain the converged κ . The raw data of thermal conductivity was averaged for each 1 ps. For each calculation of the thermal conductivity, eight independent HNEMD simulations with a total production time of 80 ns were performed (see Figs. 2 and 3). Finally, the averaged result of these eight simulations at $t = 10$ ns was taken as the values of κ .

2.2.2. EMD simulations

On the basis of fluctuation-dissipation theorem, we also calculated the thermal conductivity of planar carbon allotropes by EMD simulations together with Green-Kubo method [12,13]. This method calculates the running thermal conductivity $\kappa(t)$ by integrating the heat current autocorrelation function (HCACF) over a given correlation time t

$$\kappa(t) = \frac{1}{k_B T^2 V} \int_0^t \langle J(0)J(\tau) \rangle d\tau, \quad (2)$$

where k_B is Boltzmann's constant and $\langle J(0)J(\tau) \rangle$ is the average HCACF over different time origins with J being the heat current.

It is worth noting that the HNEMD method and EMD method are physically equivalent to each other. However, the HNEMD method enjoys much higher computational efficiency and larger signal-to-noise ratio by virtue of introducing a fictitious driving force to the system [8]. Therefore, compared with the HNEMD method, the EMD method requires more independent simulations to obtain a reliable result. As shown in Fig. 4, we carried out 80 independent simulations, each of which has a correlation time of 2 ns. The obtained 80 results were averaged to obtain the converged running thermal conductivity. All other simulation parameters in the present EMD simulations are the same as the above HNEMD simulations. For each EMD simulation, the production time was set as 20 ns that is 10 times as long as the correlation time. Therefore, each EMD result was obtained by using a total production time of 1600 ns. For all carbon allotropes, the averaged $\kappa(t)$ converges well in the time ranging from 1 ns to 2 ns. The final value of κ extracted from EMD method was obtained by averaging the results in the last 500 ps. In addition, as for κ obtained from both HNEMD and EMD methods, the corresponding standard statistical error σ_n is defined as

$$\sigma_n = \frac{\sqrt{\sum_{i=1}^n (\kappa_i - \bar{\kappa})^2}}{n}, \quad (3)$$

where n is the number of independent simulations and $\bar{\kappa}$ is the averaged thermal conductivity.

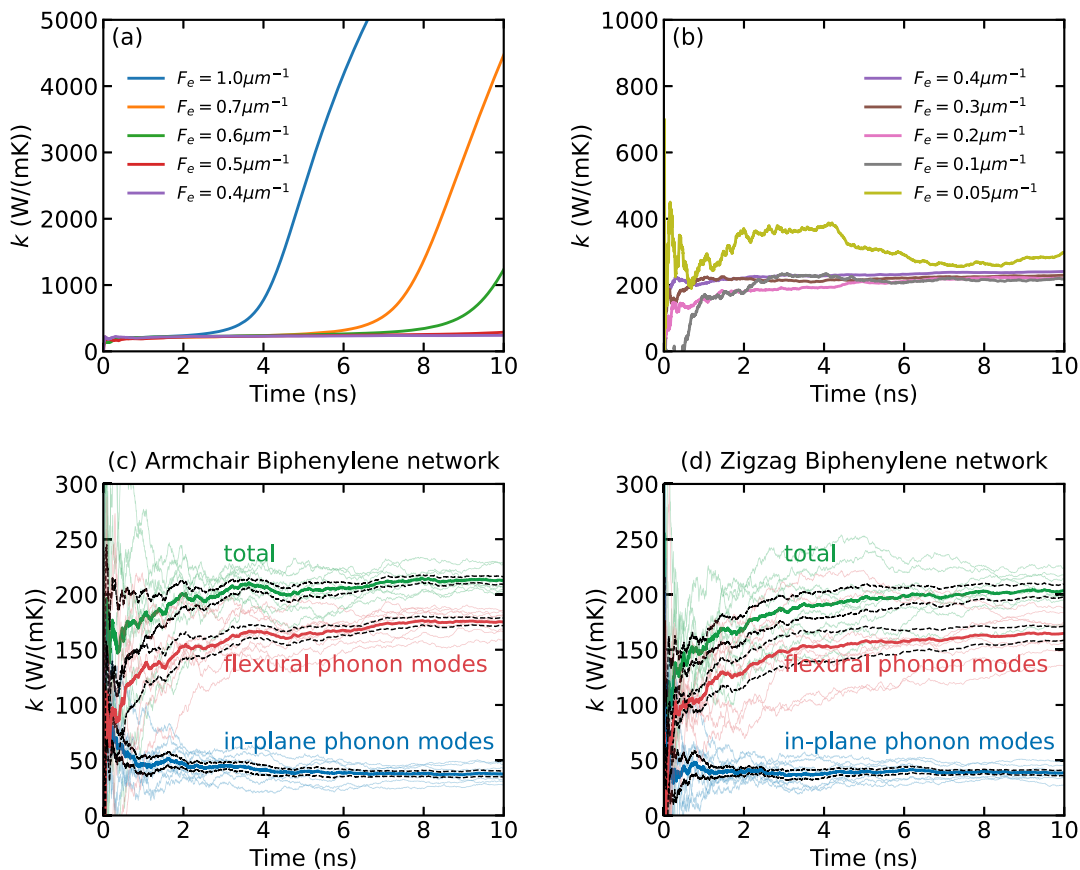


Fig. 2. Thermal conductivity of 25 nm × 25 nm biphenylene network calculated by HNEMD method at 300 K. (a and b) Results of the running thermal conductivity when F_e ranges from $0.05\ \mu\text{m}^{-1}$ to $1.0\ \mu\text{m}^{-1}$. (c and d) Total thermal conductivity (green lines) of biphenylene network along armchair and zigzag directions including contributions from in-plane (blue lines) and flexural phonon modes (red lines). Each final thermal conductivity (see solid lines) is obtained by averaging eight independent simulations (see semi-transparent lines). (For interpretation of the references to color in this figure legend, the reader is referred to the web version of this article.)

2.2.3. NEMD simulations

Both the aforementioned HNEMD and EMD methods are homogeneous methods. Thus, the size effect in them is usually trivial, which can be generally ignored. To study the thermal transport in finite-sized carbon allotropes with a length of L , we calculated the thermal conductivity κ by using NEMD simulations together with the following formula

$$\kappa(L) = \frac{Q/S}{\Delta T/L}, \quad (4)$$

where Q , ΔT , and L are the energy transfer rate, temperature difference, and effective length between the heat source and heat sink. The Langevin thermostat method was used here to control the temperature in all NEMD simulations. The corresponding time parameter in the Langevin thermostat was set as 100 fs for all carbon allotropes. In Eq. (4), S is the area of the cross section perpendicular to the transport direction. Li and coworkers [36] indicated that the nonlinear part of the temperature profile extracted from NEMD simulations should be included in the calculation of the thermal conductivity. In other words, the temperature gradient should be calculated directly as $\Delta T/L$ here instead of the slope of the linear region of the temperature profile away from the local thermostats.

Fig. 5 (a) shows the setup of NEMD simulations performed in this study. The system along the thermal transport direction, i.e., the heat flux direction was divided into three parts, including the fixed regions with the same length at two ends, two thermostats (the heat source and heat sink regions) with the same length adjacent to the fixed regions, and the thermal transport region be-

tween heat source and heat sink. The lengths of fixed regions and thermostats were set as 1 nm and 25 nm, respectively. The dimension of the sample perpendicular to the heat flux direction was set as 25 nm. As shown in Fig. 5(b), five different lengths ranging from 25 nm to 200 nm were considered for all planar carbon allotropes. Each NEMD simulation was performed for 6 ns, in which the stable temperature distribution was achieved within the initial 1 ns and the temperature gradient was obtained by averaging over the final 5 ns.

2.3. Spectral heat current analysis

Based on the NEMD and HNEMD results, the SHC analyses were further conducted to obtain the frequency-dependent MFP and length-dependent thermal conductivity. Firstly, the thermal conductivity calculated from the HNEMD method (see Eq. (1)) can be spectrally decomposed in the frequency domain as follows [8]:

$$\kappa(\omega) = \frac{2\tilde{\kappa}(\omega)}{TVF_e}. \quad (5)$$

Here, $\tilde{\kappa}(\omega)$ is the Fourier transform of the virial-velocity correlation function, which can be defined as Gabourie et al. [37]:

$$K(t) = \sum_i W_i(0) \cdot v_i(t), \quad (6)$$

where W_i and v_i denote the virial tensor and velocity of atom i , respectively. Secondly, the quasi-ballistic spectral thermal conductance $G(\omega)$ based on the NEMD results can be similarly obtained.

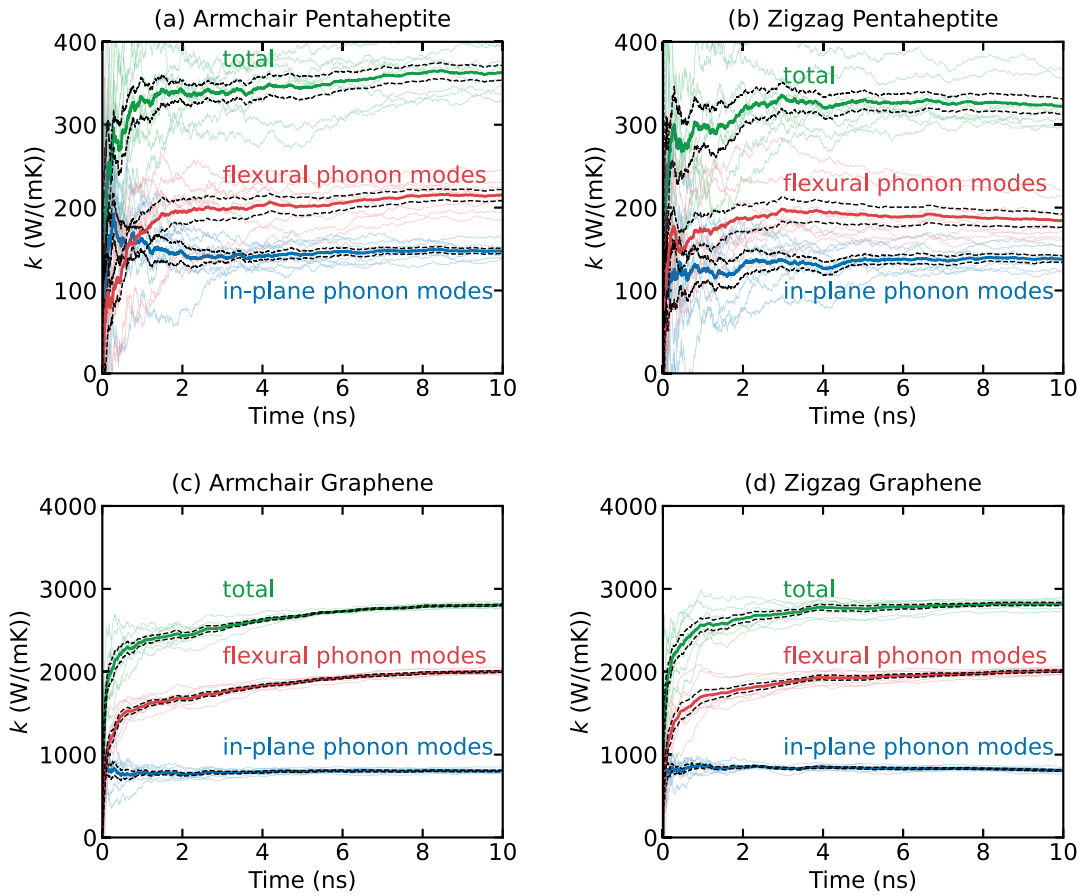


Fig. 3. Thermal conductivity (green lines) of $25\text{ nm} \times 25\text{ nm}$ (a and b) pentaheptite and (c and d) graphene calculated by HNEMD method at 300 K including contributions from in-plane (blue lines) and flexural phonon modes (red lines). Each final thermal conductivity (see solid lines) is obtained by averaging eight independent simulations (see semi-transparent lines). (For interpretation of the references to color in this figure legend, the reader is referred to the web version of this article.)

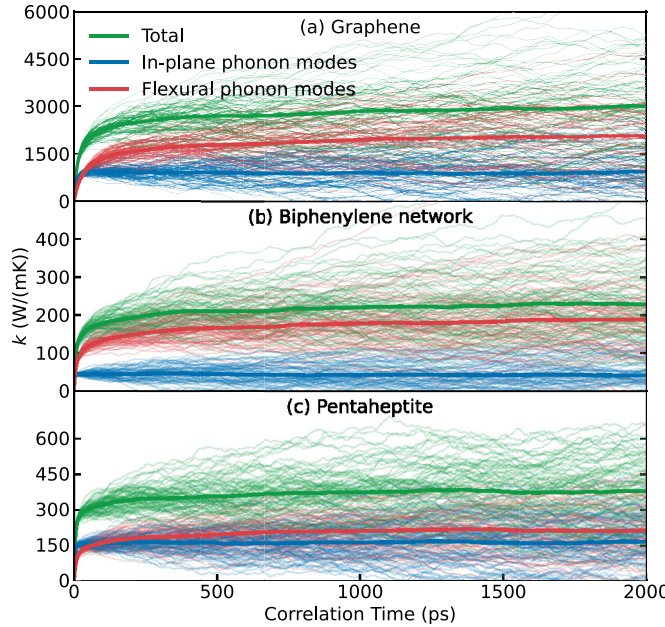


Fig. 4. Total thermal conductivity (green lines) of $25\text{ nm} \times 25\text{ nm}$ (a) graphene, (b) biphenylene network, and (c) pentaheptite calculated by EMD method at 300 K including contributions from in-plane (blue lines) and flexural phonon modes (red lines). Each final thermal conductivity (see solid lines) is obtained by averaging 80 independent simulations (see semi-transparent lines). (For interpretation of the references to color in this figure legend, the reader is referred to the web version of this article.)

Finally, the frequency-dependent MFP $\lambda(\omega)$ can be obtained from $\kappa(\omega)$ and $G(\omega)$ as follows:

$$\lambda(\omega) = \kappa(\omega)/G(\omega). \quad (7)$$

The length-dependent $\kappa(L)$ can be expressed as the following classical first-order extrapolation formula [38]:

$$\kappa(L) = \frac{\kappa_\infty}{1 + \lambda_\infty/L}, \quad (8)$$

where κ_∞ is the length-independent thermal conductivity at $1/L = 0$ and λ_∞ is the phonon MFP for the infinite system. Thus, $\kappa(L)$ can be obtained by integrating Eq. (8) in the frequency domain:

$$\kappa(L) = \int \frac{\kappa(\omega)}{1 + \lambda(\omega)/L} \frac{d\omega}{2\pi}. \quad (9)$$

Based on Eqs. (5) and (6), we obtained the HNEMD-based SHC result and NEMD-based SHC result, respectively. Based on Eqs. (7) and (9), we obtained the frequency-dependent MFP and length-dependent thermal conductivity of carbon allotropes, respectively.

2.4. First-principles calculations

First-principles calculations were conducted here to predict the lattice length, phonon dispersion relations, and electron localization function of planar carbon allotropes. All first-principles calculations were based on the Vienna Ab-initio Simulation Package (VASP) [39–41] together with the generalized gradient approximation (GGA) of the Perdew–Burke–Ernzerhof (PBE) functional form

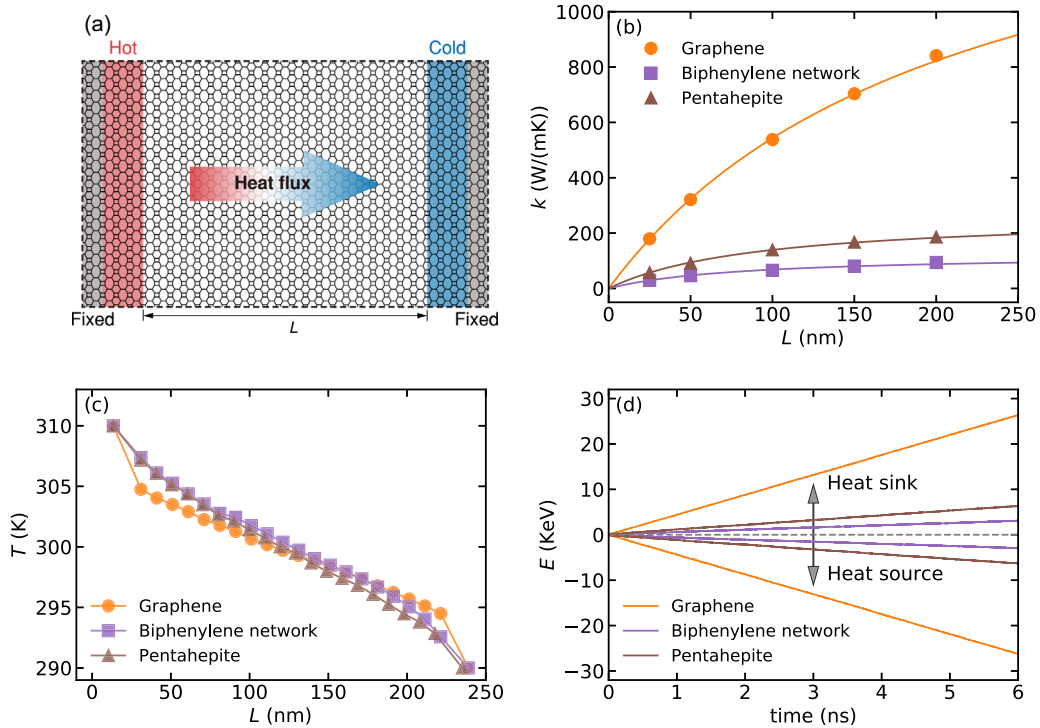


Fig. 5. The thermal conductivity of three carbon allotropes calculated by NEMD method at 300 K. (a) A schematic for the setup of NEMD simulations. (b) The length-dependent thermal conductivity $\kappa(L)$ of the carbon allotropes with an effective length L ranging from 25 nm to 500 nm. The discrete points and lines are results obtained from NEMD simulations and fitted by Eq. (5), respectively. (c) Temperature profile and (d) accumulated energy history in the armchair direction of three carbon allotropes with the same effective length of 200 nm.

for the exchange-correlation potential [42]. For the sake of comparison, we used the 2D Bravais lattices with rectangular symmetry for all three carbon allotropes as shown in Fig. S1 (see supplementary materials). The periodic boundary conditions were applied along all three Cartesian directions. A vacuum layer of 10 Å was set to avoid adjacent image-image interactions along the thickness direction. The convergence condition for the electronic self consistency loop was set as the total energy change smaller than 10^{-7} eV. The Monkhorst-Pack k -point mesh sizes for graphene, biphenylene network, and pentaheptite were set as $15 \times 9 \times 1$, $9 \times 8 \times 1$, and $6 \times 4 \times 1$, respectively. The reliability of k -point mesh sizes selected here for first-principles calculations has been verified in supplementary materials.

The structural optimization was performed by conjugate gradient method with the convergence condition for the ionic relaxation loop being the Hellmann Feynman forces smaller than 0.001 eV/Å. The second-order (harmonic) interatomic force constants were calculated by the density functional perturbation theory (DFPT) methods. First-principles-based phonon dispersion relations and the corresponding group velocities were obtained by the PHONOPY package [43] with inputs provided by the DFPT results. For the sake of comparison, the high symmetry direction of the first Brillouin zone was set as $\Gamma - X - S - Y - \Gamma$ for all carbon allotropes.

3. Results and discussion

3.1. Thermal conductivity of planar carbon allotropes

In this section, we investigate the thermal transport in graphene, biphenylene network, and pentaheptite using HNEMD, EMD, and NEMD methods. The thermal conductivities calculated by these different methods are cross-checked with each other. Ef-

forts are further made to compare the thermal transport properties of these carbon allotropes including the magnitude of thermal conductivity, the anisotropy of thermal conductivity, and the corresponding contributions of in-plane and flexural phonon modes.

We first investigate the thermal transport in biphenylene network using HNEMD simulations. Specifically, the thermal conductivity along armchair direction and zigzag direction are denoted as κ_{arm} and κ_{zig} , respectively, which are obtained from Eq. (1) by applying the driving force along the corresponding direction. As shown in Fig. 2(c and d), κ_{arm} and κ_{zig} are 213.1 ± 3.5 W/(mK) and 203.5 ± 5.8 W/(mK), respectively, indicating a very trivial anisotropy of the thermal transport in the biphenylene network. In addition, according to the heat current decomposition method proposed by Fan et al. [25], the thermal conductivity of planar carbon allotropes can be contributed by in-plane and flexural phonon branches. To measure the contribution of these two phonon modes, here we also calculate κ_{in} and κ_{flex} , which, respectively, denote the in-plane thermal conductivities of planar carbon allotropes originating from in-plane and flexural phonon modes. The thermal conductivities in the armchair and zigzag directions are averaged. Afterwards, κ_{in} and κ_{flex} in the two principle directions are similarly calculated. The results of κ_{in} and κ_{flex} are 38.1 W/(mK) and 170.2 W/(mK), respectively, which indicates that the flexural component contributes dominantly (about four-fifths) to total thermal conductivity of biphenylene network. In addition, it is also found that κ_{in} converges shortly at $t = 4$ ns in both directions, which is much faster than the κ_{flex} (converging at $t = 8$ ns).

Fig. 3 shows the running thermal conductivity of pentaheptite and graphene extracted from HNEMD simulations. The values of κ_{arm} and κ_{zig} of pentaheptite are 362.9 ± 8.5 W/(mK) and 322.4 ± 9.3 W/(mK), respectively, while the values of κ_{arm} and κ_{zig} of graphene are 2807.3 ± 11.0 W/(mK) and 2817.5 ± 18.0 W/(mK), respectively. The thermal conductivity of graphene calculated here

Table 1

Thermal conductivity (in the unit of W/(mK)) of planar carbon allotropes predicted by HNEMD and EMD methods at room temperature of 300 K.

Method	Material	κ_{arm}	κ_{zig}	κ_{in}	κ_{flex}	κ
HNEMD	Graphene	2807.3	2817.5	805.5	2007.0	2812.4
	Biphenylene network	213.1	203.5	38.1	170.2	208.3
	Pentaheptite	362.9	322.4	142.8	199.9	342.7
EMD	Graphene	3067.4	2853.2	904.1	2056.2	2960.3
	Biphenylene network	232.3	226.3	42.0	187.3	229.3
	Pentaheptite	398.9	352.4	162.9	212.8	375.7

is in good agreement with the previous studies based on HNEMD simulations such as 2847 ± 49.0 W/(mK) in Ref. [8] and 2900 ± 100.0 W/(mK) in Ref. [25]. Table 1 shows a comparison of κ_{arm} and κ_{zig} among all three carbon allotropes. It is clearly found that the anisotropy of the thermal conductivity of biphenylene network and graphene is trivial. However, κ_{arm} (362.9 W/(mK)) of pentaheptite is significantly larger than its κ_{zig} counterpart (322.4 W/(mK)), suggesting that heat current prefers to transport along the armchair direction when compared with the zigzag direction. For the sake of comparison, we further calculate the scalar thermal conductivity κ for each carbon allotrope, which has the definition of $\kappa = (\kappa_{arm} + \kappa_{zig})/2$. By comparing three carbon allotropes as listed in Table 1, we find that κ of both biphenylene network and pentaheptite is one order of magnitude lower than κ of graphene. Specifically, values of κ of both biphenylene network and pentaheptite are, respectively, only about one-thirteens and one-eights of the value of graphene. In addition, it is also found that the flexural phonon modes contribute about two-thirds of the total thermal conductivity of both graphene and pentaheptite. κ_{in} of biphenylene network having the value of 38.1 W/(mK) is much lower than 142.8 W/(mK) of pentaheptite, which results in a much lower value of κ (208.3 W/(mK)) in biphenylene network as compared to the value of 342.7 W/(mK) in pentaheptite.

The thermal conductivity of biphenylene network (208.3 W/(mK)) and pentaheptite (342.7 W/(mK)) calculated here is close to the value of 233–344 W/(mK) reported for other carbon allotropes with five-five-eight-membered rings [44], but is significantly smaller than 2013 W/(mK) of graphene-like C₃N [26] and 656 W/(mK) of hexagonal boron nitride [45]. This finding indicates that the symmetry breaking of the pristine honeycomb lattice during the structural construction of carbon allotropes with hybrid-membered rings such as biphenylene network and pentaheptite from graphene can cause a much greater reduction in the thermal conductivity than that induced by the heterogeneous elements doping or substitution.

Fig. 4 shows the running thermal conductivity of carbon allotropes as a function of the correlation time obtained by EMD simulations. The values of κ obtained from EMD simulations are 2960.3 ± 301.0 W/(mK), 229.3 ± 20.5 W/(mK), and 375.7 ± 29.0 W/(mK) for graphene, biphenylene network, and pentaheptite, respectively, which are in good agreement with the corresponding HNEMD results of 2812 ± 14.5 W/(mK), 208.3 W/(mK) ± 5.0 W/(mK), and 342.7 ± 11.3 W/(mK). Comparing the values of κ_{in} , κ_{flex} , κ_{arm} , and κ_{zig} obtained from EMD and HNEMD simulations (see Table 1), we can find that both EMD and HNEMD simulations show the similar results about the anisotropy of thermal conductivity and the contribution of phonon modes. Although the production time of 1600 ns in EMD simulations is more than one order of magnitude longer than 80 ns in HNEMD simulations, the standard error of EMD results is much larger than that of their HNEMD counterparts. This divergence reveals that the statistical accuracy of EMD simulations is far inferior to HNEMD simulations, which is consistent with the conclusions extracted from previous EMD and HNEMD studies on graphene [8], carbon nanotube [8], and C₃N [26].

The phonon scattering at the hot and cold thermostats can induce the size effect in the NEMD method. This effect can lead to a length-dependent thermal conductivity $\kappa(L)$ of the studied materials, due to the ballistic transport [46] at a small effective length L shorter than MFP. κ of all carbon allotropes with different L is graphically shown in Fig. 5(b). As defined above, here κ is calculated as the average value of κ_{arm} and κ_{zig} . As shown Fig. 5(b), κ of all carbon allotropes increases gradually with increasing L . Among all carbon allotropes considered here, graphene is found to have the largest growth rate. For example, when $L = 25$ nm, κ of graphene is 179.4 W/(mK), which is about 6 times of the value (29.3 W/(mK)) of biphenylene network and 3 times of the value (57.5 W/(mK)) of pentaheptite. However, κ of graphene with $L = 200$ nm is 841.3 W/(mK), which is about 8 times and 3.5 times larger than κ of biphenylene network (93.9 W/(mK)) and pentaheptite (186.0 W/(mK)) with the same length, respectively. Meanwhile, it is observed that κ of all carbon allotropes can be well fitted by Eq. (8), indicating that the thermal transport in all carbon allotropes now exhibits the feature of ballistic transport.

Fig. 5 (c) shows a representative temperature profile along the armchair direction of the carbon allotropes with an effective length of 200 nm. The corresponding accumulated energy evolution in the thermostats of carbon allotropes is shown in Fig. 5(d). From the temperature profile, we find a dramatic temperature drop occurring near the heat source and sink of graphene, which is attributed to the relatively larger phonon-boundary scattering when compared to biphenylene network and pentaheptite. This finding is consistent with the more significant length-dependent phenomenon observed in the thermal conductivity of graphene as shown in Fig. 5(b). After applying the linear curve fitting to the accumulated energy evolution curves, we obtain the energy transfer rates of graphene, biphenylene network, and pentaheptite as 4.38 eV/ps, 0.49 eV/ps, and 1.03 eV/ps, respectively, which are consistent with the magnitudes of their thermal conductivity. In addition, through comparing κ_{arm} and κ_{zig} extracted from NEMD simulations, we also investigate the anisotropy of thermal transport in finite-sized carbon allotropes as shown in Fig. S8 (see supplementary materials). It is observed that κ_{arm} is very close to κ_{zig} in graphene and biphenylene network, indicating an isotropic thermal transport property of these materials. As for pentaheptite, the difference between κ_{arm} and κ_{zig} is found to increase as L grows. In other words, the anisotropy of thermal transport in pentaheptite will become more significant with increasing L , which is consistent with the HNEMD and NEMD results as shown in Table 1.

3.2. Phonon property analysis

According to the classical phonon-gas model, the phonon conductivity can be expressed as

$$\kappa = \frac{1}{3} C_V v_g \lambda, \quad (10)$$

where C_V , v_g , and λ are the volumetric heat capacity, phonon group velocity, and phonon MFP, respectively. According to our results, it can be clearly found that the thermal transport property of both

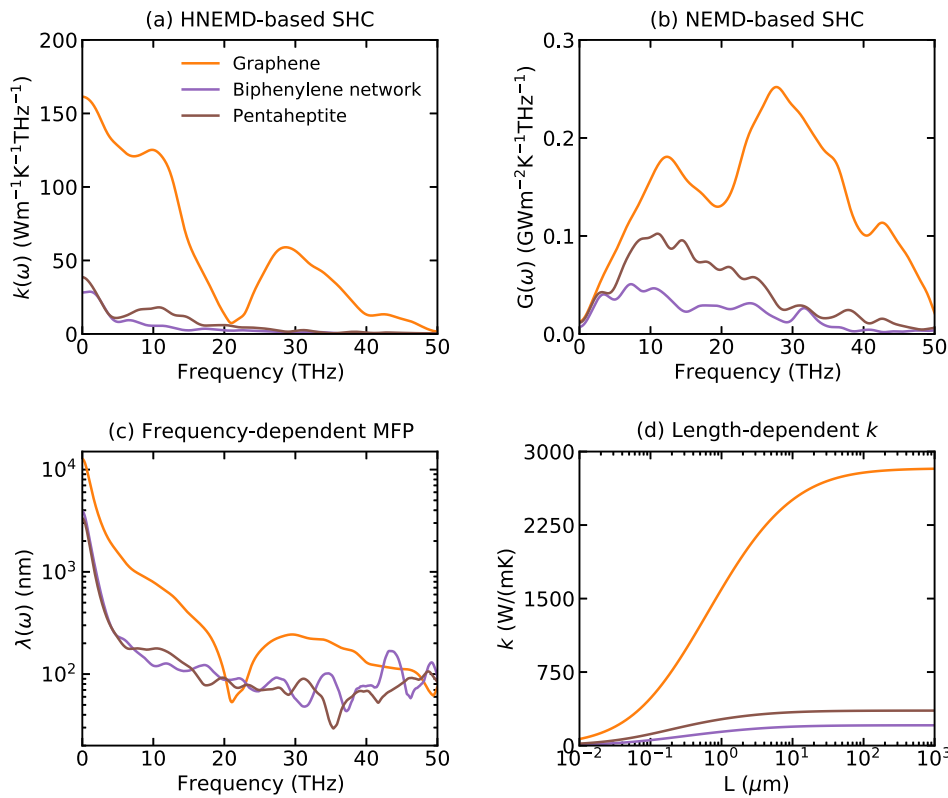


Fig. 6. A comparison of SHC results of three carbon allotropes at 300 K. (a) The spectral thermal conductivity $k(\omega)$ based on HNEMD results. (b) The spectral ballistic thermal conductance $G(\omega)$ based on NEMD results. (c) The frequency-dependent MFP $\lambda(\omega)$ obtained by Eq. (7). (d) The length-dependent thermal conductivity k obtained by Eq. (9).

biphenylene network and pentaheptite is much weaker than that of graphene. In this section, the analysis of phonon properties including the group velocity and MFP is performed to reveal the origin of the difference observed in the thermal conductivity of three carbon allotropes. Specifically, the frequency-dependent MFP is obtained by SHC calculations based on HNEMD and NEMD results, while the group velocity is calculated by lattice dynamics methods. In addition, the vibrational density of states (VDOS) is also calculated to provide more information on the vibrational modes of carbon allotropes.

Fig. 6 shows SHC results including spectral thermal conductivity $\kappa(\omega)$, spectral ballistic thermal conductance $G(\omega)$, frequency-dependent MFP $\lambda(\omega)$, and length-dependent thermal conductivity $\kappa(L)$ of three carbon allotropes. The corresponding SHC results originating from in-plane and flexural phonon modes are shown in Figs. S9 and S10 (see supplementary materials). Here, all SHC results shown here are obtained by averaging results in armchair and zigzag directions. From Fig. 6(a), we can see that κ of all carbon allotropes is mainly attributed to the phonon modes less than 20 THz, which is especially significant in the biphenylene network and pentaheptite. As shown in Fig. S9, κ of graphene and pentaheptite is mainly contributed by the flexural phonon modes. For the biphenylene network, the dominant contribution of flexural phonon modes to κ dominated becomes more significant. This finding is consistent with the previous HNEMD and EMD results that the flexural phonon modes of biphenylene network contribute about four-fifths of its thermal conductivity, while flexural phonon modes contribute two-thirds of the thermal conductivity of both graphene and pentaheptite. After combined with $G(\omega)$ obtained by NEMD-based SHC (see Fig. 6(b)), the spectral phonon MFP $\lambda(\omega)$ can be obtained by Eq. (7) (see Fig. 6(c)). It is found that at the extreme condition that $\omega \rightarrow 0$, the values

of λ_{\max} of graphene, biphenylene network, and pentaheptite are around 10,000 nm, 4000 nm, and 4000 nm, respectively. With a choice of $F_e = 0.1 \mu\text{m}^{-1}$ in HNEMD simulations, λ_{\max} is in accordance with the criteria $F_e \lambda_{\max} \lesssim 1$, which further ensures that HNEMD simulations are now in the linear response regime [8]. It is also clearly observed that λ of graphene is much larger than that of biphenylene and pentaheptite at a low frequency smaller than 20 THz, which is consistent with the fact that graphene possesses the largest thermal conductivity among three carbon allotropes.

Ultimately, as shown in Fig. 6(d), κ of graphene, biphenylene, and pentaheptite converges to 2785.1 W/(mK), 210.0 W/(mK), and 386.0 W/(mK), respectively, when L is approaching 1 mm, which agree well with our previous HNEMD and EMD results (see Table 1). The minimum length corresponding to the onset of the convergence of κ is in the scale of millimeter, which indicates that the NEMD simulation is a computationally expensive method in obtaining a convergence value of κ for 2D carbon allotropes. Based on NEMD simulations together with the extrapolation method, in the previous study [18], 2272.0 W/(mK) and 156.5 W/(mK) were, respectively, predicted for κ of graphene and biphenylene network, which are much smaller than our results of 2812.4 W/(mK) and 208.3 W/(mK) obtained by HNEMD method here. This large gap observed in the results obtained from the present and previous studies can be mainly attributed to the fact that the length smaller than 100 nm used in the previous study is too short to predict a reliable thermal conductivity in the extrapolation method. In Tab. S1 (see the supplementary materials), we further compare the thermal conductivity predicted from the present work with the result previously obtained from various methods including MD-based methods (HNEMD, EMD, and NEMD) and BTE methods. As detailed in the related discussion in supplementary materials, the present results are generally consistent with the results reported in previ-

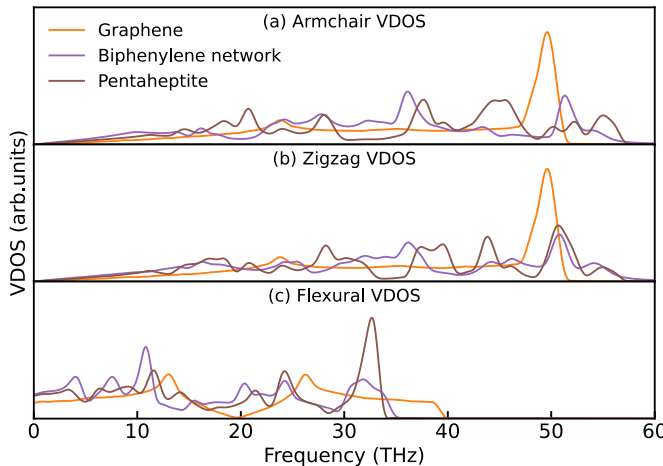


Fig. 7. A comparison of VDOS of graphene, biphenylene network, and pentaheptite. Three components including (a) armchair VDOS, (b) zigzag VDOS, and (c) flexural VDOS are considered here.

ous studies. In addition, as shown in Fig. S10 (see supplementary materials), the flexural phonon modes are found to contribute the major part of $\lambda(\omega)$ and $k(L)$ in all carbon allotropes, which is consistent with the results extracted from the above $\kappa(\omega)$.

To better understand the thermal transport in carbon allotropes considered in this study, the VDOS is calculated by performing the following Fourier integral transform on the atomic velocity autocorrelation function (VACF) [47]:

$$\text{VDOS}(\omega) = \int \left\langle \sum_j v_j(0) \cdot v_j(t) \right\rangle e^{-2\pi i \omega t} dt, \quad (11)$$

where σ is the frequency, i is the imaginary unit, and $\langle \sum_j v_j(0) \cdot v_j(t) \rangle$ is the VACF. Here, $v_j(0)$ and $v_j(t)$ are velocities of the j th atom at time t and the initial time, respectively. Considering the planar feature of carbon allotropes considered here, their VDOS is further decomposed into three components, respectively, in armchair, zigzag, and flexural (out-of-plane) directions.

The armchair, zigzag, and flexural components of VDOS in three carbon allotropes are shown in Fig. 7. As for all VDOS components, more peaks and modes are observed in biphenylene network and pentaheptite when compared with graphene. This difference is attributed to the fact that more atoms exist in the Bravais lattice of biphenylene network and pentaheptite, because the symmetry is greatly reduced after the structural transformation of biphenylene network and pentaheptite from graphene (see Fig. 1). As for the armchair and zigzag VDOS components, the sharp peak around the high frequency of 50 THz in graphene dis-

appears in the result of biphenylene network. Based on the aforementioned SHC results, it is found that the thermal conductivity of carbon allotropes is mainly attributed to the flexural phonon modes with a low frequency smaller than 20 THz. In the flexural VDOS with the frequency smaller than 20 THz (see Fig. 7(c)), the peaks of both biphenylene network and pentaheptite locate in the frequency region lower than that of graphene. In addition, the flexural VDOS in this region of biphenylene network and pentaheptite show more peaks (corresponding to more phonon modes) when compared with the corresponding result of graphene. This difference observed in the flexural VDOS of biphenylene network and pentaheptite indicates a stronger phonon-phonon scattering effect and correspondingly a shorter phonon lifetime in biphenylene network and pentaheptite, which is a factor responsible for the much weaker thermal transport property observed in biphenylene network and pentaheptite when compared with that of graphene. A further comparison among the armchair VDOS, zigzag VDOS, and flexural VDOS of each carbon allotrope is shown in Fig. S11 (see supplementary materials). It is found that the armchair VDOS and zigzag VDOS in graphene are identical to each other very well. Similarly, the armchair VDOS in biphenylene network is very close to its zigzag VDOS. However, the armchair VDOS in pentaheptite is clearly found to be different with its zigzag VDOS, which is consistent with its anisotropic thermal transport property as shown in Table 1.

The aforementioned SHC analysis suggests that the phonon MFP of graphene is much longer than that of two other carbon allotropes, which is an important factor responsible for the much higher thermal conductivity observed in graphene. In addition to the phonon MFP, as suggested by the classical phonon-gas model in Eq. (10), the phonon group velocity is another important parameter determining the lattice thermal conductivity. Thus, we show the phonon dispersion curves of three carbon allotropes obtained by lattice dynamics calculations in Fig. 8 and further compare their phonon group velocities in Fig. 9. For the sake of comparison, the high symmetry direction of the first Brillouin zone is set as $\Gamma - X - S - Y - \Gamma$ for all carbon allotropes. Among three acoustic modes, the longitudinal acoustic (LA) and transverse acoustic (TA) modes of all carbon allotropes show linear dispersion, while their flexural acoustic (ZA) mode shows a quadratic dispersion, which is a classical characteristic of phonon dispersion curves of monolayer 2D materials [27]. It is found that the frequency corresponding to the acoustic modes of graphene locates much higher than that of biphenylene network and pentaheptite. For example, at the X point, frequencies at LA, TA, and ZA modes of graphene are, respectively, around 33 THz, 26 THz, and 13 THz, which are much larger than the corresponding results of biphenylene network (24 THz, 6 THz, and 4 THz) and pentaheptite (16 THz, 11 THz, and 2 THz). The speed of sound equaling to the slope of all three acoustic

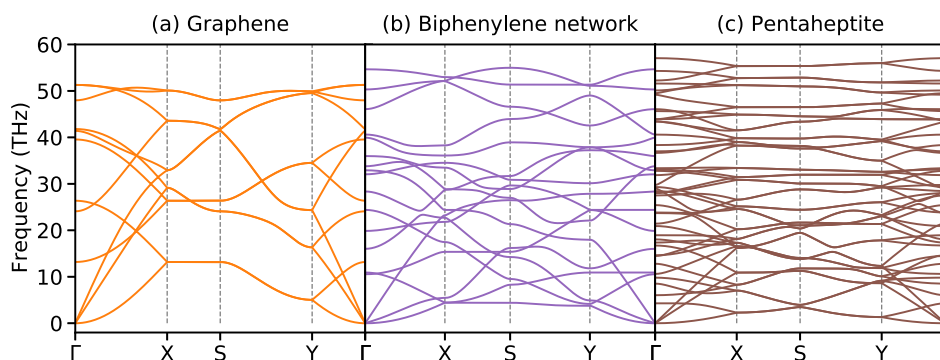


Fig. 8. The phonon dispersion curves of (a) graphene, (b) biphenylene network, and (c) pentaheptite along high symmetry directions of the first Brillouin zone.

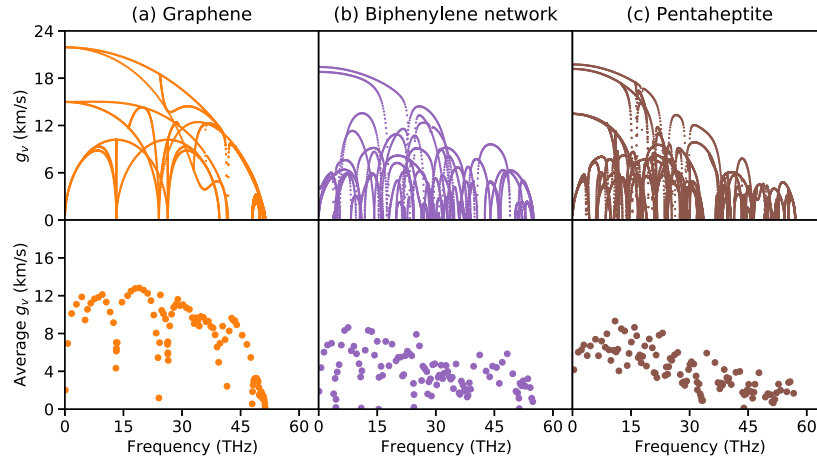


Fig. 9. A comparison of the phonon group velocity g_v and the corresponding average group velocity of (a) graphene, (b) biphenylene network, and (c) pentaheptite. The averaged g_v is obtained by averaging the group velocity each 1 THz.

modes in biphenylene network and pentaheptite is found to be much smaller than that in graphene. This difference is directly related to the different group velocities observed among three carbon allotropes as shown in Fig. 9.

From Fig. 9, it can be obviously observed that the average group velocity of biphenylene network and pentaheptite is significantly smaller than that of graphene at the low frequency region smaller than 20 THz that mainly contributes to the thermal conductivity. The highest value of average group velocity is found to decrease from 12.0 km/s of graphene to 8.9 km/s of biphenylene network and 9.1 km/s of pentaheptite, which indicates a weaker phonon transport property and correspondingly a much lower thermal conductivity of biphenylene network and pentaheptite when compared to graphene. Although biphenylene network and pentaheptite have almost the same highest value of average

group velocity, the group velocity of biphenylene network within the low frequency smaller than 15 THz is much smaller than that of pentaheptite, leading to a much lower thermal conductivity of 208.3 W/(mK) when compared with 342.7 W/(mK) of pentaheptite.

3.3. Electron density and mechanical properties

In the above discussion, we have demonstrated that the phonon MFP and group velocity of biphenylene network and pentaheptite are significantly smaller than those of graphene, leading to a much weaker thermal transport property observed in biphenylene network and pentaheptite. Furthermore, although the phonon MFP of biphenylene network is close to that of pentaheptite, the biphenylene network has a group velocity smaller than that of pentaheptite.

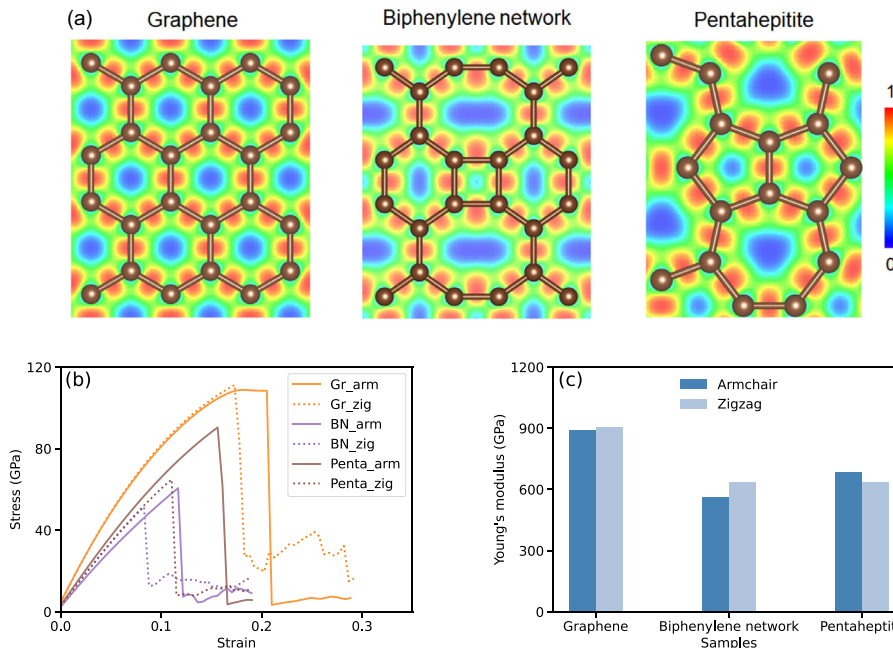


Fig. 10. (a) The ELF of graphene, biphenylene network, and pentaheptite. For clarify, $3 \times 2 \times 1$ supercell, $3 \times 2 \times 1$ supercell, and unit cell are presented for graphene, biphenylene network, and pentaheptite, respectively. The ELF is visualized by using VESTA package [48]. (b) Stress-strain response of graphene, biphenylene network, and pentaheptite uniaxially elongated along armchair and zigzag directions. In the legend, Gr, BN, and Penta are respectively short for graphene, biphenylene network, and pentaheptite, while arm and zig respectively denote the tensile simulation along armchair direction and zigzag direction. (c) The corresponding Young's modulus obtained from tensile simulations.

site. Thus, among three carbon allotropes, the lowest thermal conductivity is observed in biphenylene network. To reveal the origin of the significant reduction in phonon MFP and group velocity of biphenylene network and pentaheptite, the electron localization function (ELF) [49] of all carbon allotropes is graphically plotted in Fig. 10(a) to illustrate their atomic bonding features. It is found that the electron localization occurs around the center of all bonds in three carbon allotropes, which, as expected, clearly indicates the dominance of covalent bonding. However, the electron localization of biphenylene network prefers to locate in the space of eight-membered and six-membered rings and deviates from the four-membered rings. A similar distribution is also found in pentaheptite, in which the electron localization prefers to locate in the seven-membered rings rather than five-membered rings. The deviation degree of electron localization in biphenylene is greater than that in pentaheptite, while no deviation is found in graphene due to its perfect symmetry structure with six-membered rings. This can be explained by the difference in structural symmetry of studied carbon allotropes. For example, the inner space of four-membered rings in biphenylene is much smaller than that of its six-membered and eight-membered rings. As a result, the electron localization moves to the six-membered and eight-membered rings due to the repulsion force between electrons in a small space. The similar mechanism is also applicable for the five-membered and seven-membered rings in pentaheptite. The deviation of electronic localization found in biphenylene network and pentaheptite indicates stronger bond anharmonicity [50], leading to stronger phonon scattering, lower phonon MFP and correspondingly weaker thermal transport property when compared with graphene.

We further performed MD simulations-based uniaxial tensile test on three carbon allotropes to extract their mechanical properties (see supplementary materials for simulation details). Fig. 10(b) shows the stress-strain curves of three carbon allotropes along armchair and zigzag directions. The corresponding Young's modulus was obtained through performing the linear curve fitting to the stress-strain curves with the strain smaller than 0.05. Among these carbon allotropes, graphene is found to possess the largest strength and Young's modulus, followed by pentaheptite and biphenylene network. This trend is consistent with their thermal conductivity. The Young's moduli of graphene, biphenylene network, and pentaheptite in the armchair direction are 892.5 GPa, 563.5 GPa, and 683.8 GPa, respectively, while their values in the zigzag direction are 903.4 GPa, 632.7 GPa, and 634.7 GPa, respectively (see Fig. 10(c)). Based on the ELF analysis together with the calculated mechanical properties of various carbon allotropes, we can see that due to the reduction in the structural symmetry of biphenylene network and pentaheptite, their bond property and mechanical properties are different from those of graphene, which leads to the lower phonon group velocity and MFP observed in biphenylene network and pentaheptite. These differences finally result in the weaker phonon transport property observed in biphenylene network and pentaheptite.

4. Conclusion

In conclusion, the thermal transport in three planar sp^2 -hybridized carbon allotropes including graphene, biphenylene network, and pentaheptite is investigated in this study by MD simulations together first-principles calculations. Three MD-based methods, i.e., HNEMD, EMD, and NEMD are employed to obtain a reliable prediction of the thermal conductivity of these carbon allotropes. According to our HNEMD results, the thermal conductivities of biphenylene network and pentaheptite are 208.3 W/(mK) and 342.7 W/(mK), respectively, which are only one-thirteenth and one-eighth of the value (2812.4 W/(mK)) of graphene. The much smaller thermal conductivity observed in biphenylene network and

pentaheptite originates from the symmetry breaking of the pristine honeycomb lattice during the structural transformation from graphene to biphenylene network and pentaheptite. The results obtained from EMD and NEMD simulations are in good agreement with those from HNEMD simulations, which, to some extent, proves the reliability of results predicted from the present calculations. In addition, it is also found that the thermal conductivity of all three carbon allotropes is mainly attributed to the flexural phonon modes. Especially for biphenylene network, the flexural phonon contributes up to four-fifths of the total thermal conductivity. The SHC analysis and lattice dynamics analysis demonstrate that both the phonon group velocity and MFP of biphenylene network and pentaheptite are much smaller than those of graphene. Furthermore, the deviation of ELF found in biphenylene network and pentaheptite indicates that the bond property of these two carbon allotropes is different from that of graphene, which results in a larger anharmonicity and stronger phonon-phonon scattering in them when compared those of graphene. This mechanism is further proved through the different mechanical properties observed among these three carbon allotropes. Our study not only provides a deep understanding of fundamental mechanisms of phonon transport in 2D carbon allotropes, but also facilitates their applications as carbon nanodevices.

Declaration of Competing Interest

Authors declare that they have no conflict of interest.

CRediT authorship contribution statement

Penghua Ying: Conceptualization, Methodology, Software, Formal analysis, Investigation, Writing – original draft. **Ting Liang:** Methodology, Software, Formal analysis, Writing – review & editing. **Yao Du:** Software, Formal analysis, Visualization. **Jin Zhang:** Conceptualization, Formal analysis, Writing – original draft. **Xiaoliang Zeng:** Formal analysis, Resources. **Zheng Zhong:** Conceptualization, Supervision, Funding acquisition, Writing – review & editing.

Acknowledgments

This study was supported by the National Key R&D Program of China (No. 2018YFB1502602) and the National Natural Science Foundation of China (Nos. 11932005 and 11772106). The authors thank Mr. Xin Wu and Mr. Qiangqiang Ma for discussions and insightful comments.

Supplementary material

Supplementary material associated with this article can be found, in the online version, at doi:[10.1016/j.ijheatmasstransfer.2021.122060](https://doi.org/10.1016/j.ijheatmasstransfer.2021.122060).

References

- [1] K.S. Novoselov, A.K. Geim, S.V. Morozov, D. Jiang, Y. Zhang, S.V. Dubonos, I.V. Grigorieva, A.A. Firsov, Electric field effect in atomically thin carbon films, *Science* 306 (5696) (2004) 666–669.
- [2] C. Lee, X. Wei, J.W. Kysar, J. Hone, Measurement of the elastic properties and intrinsic strength of monolayer graphene, *Science* 321 (5887) (2008) 385–388.
- [3] A.A. Balandin, S. Ghosh, W. Bao, I. Calizo, D. Teweldebrhan, F. Miao, C.N. Lau, Superior thermal conductivity of single-layer graphene, *Nano Lett.* 8 (3) (2008) 902–907.
- [4] S. Chen, A.L. Moore, W. Cai, J.W. Suk, J. An, C. Mishra, C. Amos, C.W. Magnuson, J. Kang, L. Shi, et al., Raman measurements of thermal transport in suspended monolayer graphene of variable sizes in vacuum and gaseous environments, *ACS Nano* 5 (1) (2011) 321–328.
- [5] G.R. Bhimanapati, Z. Lin, V. Meunier, Y. Jung, J. Cha, S. Das, D. Xiao, Y. Son, M.S. Strano, V.R. Cooper, et al., Recent advances in two-dimensional materials beyond graphene, *ACS Nano* 9 (12) (2015) 11509–11539.

- [6] G. Li, Y. Li, H. Liu, Y. Guo, Y. Li, D. Zhu, Architecture of graphdiyne nanoscale films, *Chem. Commun.* 46 (19) (2010) 3256–3258.
- [7] Q. Fan, L. Yan, M.W. Tripp, O. Krejčí, S. Dimosthenous, S.R. Kachel, M. Chen, A.S. Foster, U. Koert, P. Liljeroth, et al., Biphenylene network: a nonbenzenoid carbon allotrope, *Science* 372 (6544) (2021) 852–856.
- [8] Z. Fan, H. Dong, A. Harju, T. Ala-Nissila, Homogeneous nonequilibrium molecular dynamics method for heat transport and spectral decomposition with many-body potentials, *Phys. Rev. B* 99 (6) (2019) 064308.
- [9] X. Yang, J. Dai, Y. Zhao, S. Meng, Phonon thermal transport in a class of graphene allotropes from first principles, *Phys. Chem. Chem. Phys.* 20 (23) (2018) 15980–15985.
- [10] S. Zhang, J. Zhou, Q. Wang, X. Chen, Y. Kawazoe, P. Jena, Penta-graphene: a new carbon allotrope, *Proc. Natl. Acad. Sci.* 112 (8) (2015) 2372–2377.
- [11] F.Q. Wang, J. Yu, Q. Wang, Y. Kawazoe, P. Jena, Lattice thermal conductivity of penta-graphene, *Carbon* 105 (2016) 424–429.
- [12] M.S. Green, Markoff random processes and the statistical mechanics of time-dependent phenomena. ii. irreversible processes in fluids, *J. Chem. Phys.* 22 (3) (1954) 398–413.
- [13] R. Kubo, Statistical-mechanical theory of irreversible processes. I. General theory and simple applications to magnetic and conduction problems, *J. Phys. Soc. Jpn.* 12 (6) (1957) 570–586.
- [14] C. Su, H. Jiang, J. Feng, Two-dimensional carbon allotrope with strong electronic anisotropy, *Phys. Rev. B* 87 (7) (2013) 075453.
- [15] X. Li, Q. Wang, P. Jena, ψ -graphene: a new metallic allotrope of planar carbon with potential applications as anode materials for lithium-ion batteries, *J. Phys. Chem. Lett.* 8 (14) (2017) 3234–3241.
- [16] S. Wang, B. Yang, H. Chen, E. Ruckenstein, Popgraphene: a new 2D planar carbon allotrope composed of 5–8–5 carbon rings for high-performance lithium-ion battery anodes from bottom-up programming, *J. Mater. Chem. A* 6 (16) (2018) 6815–6821.
- [17] M. Liu, M. Liu, L. She, Z. Zha, J. Pan, S. Li, T. Li, Y. He, Z. Cai, J. Wang, et al., Graphene-like nanoribbons periodically embedded with four-and eight-membered rings, *Nat. Commun.* 8 (1) (2017) 1–7.
- [18] H. Dong, Z. Zhang, Z. Feng, J. Kang, D. Wu, Q. Wang, J. Li, R. Su, Origins of low lattice thermal conductivity in 2Dcarbon allotropes, *J. Mater. Res. Technol.* 11 (2021) 1982–1990.
- [19] V.H. Crespi, L.X. Benedict, M.L. Cohen, S.G. Louie, Prediction of a pure-carbon planar covalent metal, *Phys. Rev. B* 53 (20) (1996) R13303.
- [20] L. Lindsay, D. Brodo, Optimized Tersoff and Brenner empirical potential parameters for lattice dynamics and phonon thermal transport in carbon nanotubes and graphene, *Phys. Rev. B* 81 (20) (2010) 205441.
- [21] Z. Fan, L.F.C. Pereira, H.-Q. Wang, J.-C. Zheng, D. Donadio, A. Harju, Force and heat current formulas for many-body potentials in molecular dynamics simulations with applications to thermal conductivity calculations, *Phys. Rev. B* 92 (9) (2015) 094301.
- [22] Z. Fan, W. Chen, V. Vierimaa, A. Harju, Efficient molecular dynamics simulations with many-body potentials on graphics processing units, *Comput. Phys. Commun.* 218 (2017) 10–16.
- [23] W.C. Swope, H.C. Andersen, P.H. Berens, K.R. Wilson, A computer simulation method for the calculation of equilibrium constants for the formation of physical clusters of molecules: application to small water clusters, *J. Chem. Phys.* 76 (1) (1982) 637–649.
- [24] S. Plimpton, Fast parallel algorithms for short-range molecular dynamics, *J. Comput. Phys.* 117 (1) (1995) 1–19.
- [25] Z. Fan, L.F.C. Pereira, P. Hirvonen, M.M. Ervasti, K.R. Elder, D. Donadio, T. Ala-Nissila, A. Harju, Thermal conductivity decomposition in two-dimensional materials: application to graphene, *Phys. Rev. B* 95 (14) (2017) 144309.
- [26] X. Wu, Q. Han, Thermal transport in pristine and defective two-dimensional polyaniline (C3N), *Int. J. Heat Mass Transf.* 173 (2021) 121235.
- [27] B. Mortazavi, M. Shahrokhi, M. Raeisi, X. Zhuang, L.F.C. Pereira, T. Rabczuk, Outstanding strength, optical characteristics and thermal conductivity of graphene-like BC₃ and BC₆N semiconductors, *Carbon* 149 (2019) 733–742.
- [28] B. Mortazavi, Ultra high stiffness and thermal conductivity of graphene like C3N, *Carbon* 118 (2017) 25–34.
- [29] B. Mortazavi, Ultrahigh thermal conductivity and strength in direct-gap semiconducting graphene-like bc₆n: a first-principles and classical investigation, *Carbon* 182 (2021) 373–383.
- [30] S.J. Stuart, A.B. Tutein, J.A. Harrison, A reactive potential for hydrocarbons with intermolecular interactions, *J. Chem. Phys.* 112 (14) (2000) 6472–6486.
- [31] K. Chenoweth, A.C. Van Duin, W.A. Goddard, Reaxff reactive force field for molecular dynamics simulations of hydrocarbon oxidation, *J. Phys. Chem. A* 112 (5) (2008) 1040–1053.
- [32] D.J. Evans, Homogeneous NEMD algorithm for thermal conductivity—Application of non-canonical linear response theory, *Phys. Lett. A* 91 (9) (1982) 457–460.
- [33] Z. Yao, J.-S. Wang, B. Li, G.-R. Liu, Thermal conduction of carbon nanotubes using molecular dynamics, *Phys. Rev. B* 71 (8) (2005) 085417.
- [34] K.K. Mandadapu, R.E. Jones, P. Papadopoulos, A homogeneous nonequilibrium molecular dynamics method for calculating thermal conductivity with a three-body potential, *J. Chem. Phys.* 130 (20) (2009) 204106.
- [35] B. Dongre, T. Wang, G.K. Madsen, Comparison of the Green–Kubo and homogeneous non-equilibrium molecular dynamics methods for calculating thermal conductivity, *Modell. Simul. Mater. Sci. Eng.* 25 (5) (2017) 054001.
- [36] Z. Li, S. Xiong, C. Sievers, Y. Hu, Z. Fan, N. Wei, H. Bao, S. Chen, D. Donadio, T. Ala-Nissila, Influence of thermostating on nonequilibrium molecular dynamics simulations of heat conduction in solids, *J. Chem. Phys.* 151 (23) (2019) 234105.
- [37] A.J. Gabourie, Z. Fan, T. Ala-Nissila, E. Pop, Spectral decomposition of thermal conductivity: comparing velocity decomposition methods in homogeneous molecular dynamics simulations, *Phys. Rev. B* 103 (20) (2021) 205421.
- [38] P.K. Schelling, S.R. Phillpot, P. Kebinski, Comparison of atomic-level simulation methods for computing thermal conductivity, *Phys. Rev. B* 65 (14) (2002) 144306.
- [39] G. Kresse, J. Furthmüller, Efficiency of ab-initio total energy calculations for metals and semiconductors using a plane-wave basis set, *Comput. Mater. Sci.* 6 (1) (1996) 15–50.
- [40] G. Kresse, J. Furthmüller, Efficient iterative schemes for ab initio total-energy calculations using a plane-wave basis set, *Phys. Rev. B* 54 (16) (1996) 11169.
- [41] G. Kresse, D. Joubert, From ultrasoft pseudopotentials to the projector augmented-wave method, *Phys. Rev. B* 59 (3) (1999) 1758.
- [42] J.P. Perdew, K. Burke, M. Ernzerhof, Generalized gradient approximation made simple, *Phys. Rev. Lett.* 77 (18) (1996) 3865.
- [43] A. Togo, I. Tanaka, First principles phonon calculations in materials science, *Scr. Mater.* 108 (2015) 1–5.
- [44] S. Li, H. Ren, Y. Zhang, X. Xie, K. Cai, C. Li, N. Wei, Thermal conductivity of two types of 2D carbon allotropes: a molecular dynamics study, *Nanoscale Res. Lett.* 14 (1) (2019) 1–11.
- [45] X. Wu, Q. Han, Thermal conductivity of monolayer hexagonal boron nitride: from defective to amorphous, *Comput. Mater. Sci.* 184 (2020) 109938.
- [46] K. Sääskilahti, J. Oksanen, S. Volz, J. Tulkki, Frequency-dependent phonon mean free path in carbon nanotubes from nonequilibrium molecular dynamics, *Phys. Rev. B* 91 (11) (2015) 115426.
- [47] J. Dickey, A. Paskin, Computer simulation of the lattice dynamics of solids, *Phys. Rev.* 188 (3) (1969) 1407.
- [48] K. Momma, F. Izumi, Vesta 3 for three-dimensional visualization of crystal, volumetric and morphology data, *J. Appl. Crystallogr.* 44 (6) (2011) 1272–1276.
- [49] B. Silvi, A. Savin, Classification of chemical bonds based on topological analysis of electron localization functions, *Nature* 371 (6499) (1994) 683–686.
- [50] X. Wu, V. Varshney, J. Lee, T. Zhang, J.L. Wohlgend, A.K. Roy, T. Luo, Hydrogenation of penta-graphene leads to unexpected large improvement in thermal conductivity, *Nano Lett.* 16 (6) (2016) 3925–3935.